第 34 卷第 6 期
2018 年 6 月

无 机 化 学 学 报
CHINESE JOURNAL OF INORGANIC CHEMISTRY

Vol.34 No.6
1127-1136

单锰取代的 Keggin 型多酸吸附大气小分子 X(X=H_2O, N_2, O_2, NO, N_2O, CO 和 CO_2)的密度泛函理论计算研究

刘春光* 张含玉 蒋梦绪
(东北电力大学化学工程学院,吉林 132012)

摘要: 基于密度泛函理论(DFT)M06L 方法对一系列单锰取代的 Keggin 型 POM 吸附大气小分子 X (X=H_2O, N_2, O_2, NO, N_2O, CO 和 CO_2)配合物的分子几何,电子结构和成键性质进行了系统研究。由于 POM 的多阴离子性质,铯盐 $Cs_4[PW_{11}O_{39}Mn^{Ⅲ}H_2O]$被用来考虑抗衡离子效应。DFT-M06L 计算表明,当改变 4 个 Cs 抗衡阳离子的位置时,多酸阴离子的几何结构和电子结构参数几乎没有变化。当不考虑抗衡离子效应,在气相和溶液中单独优化多酸阴离子($[PW_{11}O_{39}Mn^{Ⅲ}H_2O]^{4-}$)时,其主要几何和电子参数没有显著变化。比较不同自旋态的能量表明$[PW_{11}O_{39}Mn^{Ⅱ}X]^{4-}$(X=$H_2O$、$N_2$、$N_2O$、CO 和 CO_2)的最低能量态是高自旋五重态,$[PW_{11}O_{39}Mn^{Ⅲ}O_2]^{4-}$为三重态, 而 $[PW_{11}O_{39}Mn^{Ⅲ}NO]^{4-}$则为双重态。这些大气小分子在类卟啉 POM 配体上的吸附能量按照以下顺序增加:$N_2<N_2O<CO\approx CO_2<O_2<H_2O<NO$。POM-Mn-NO 配合物具有较大的吸附能。Mulliken 布居分析表明,NO 配体与多酸中 $Mn^{Ⅲ}$ 中心的相互作用主要来自于中间自旋态的 $Mn^{Ⅲ}$中心与 $NO^{·}$ 分子之间的反铁磁性耦合相互作用。

关键词: 密度泛函理论; 电子结构; 多金属氧酸盐; 大气小分子
中图分类号: O641.12; O611.65 **文献标识码**: A **文章编号**: 1001-4861(2018)06-1127-10
DOI:10.11862/CJIC.2018.143

DFT Study of Mono-Manganese-Substituted Keggin-Type Polyoxometalates with Atmospheric Small Molecules X (X=H_2O, N_2, O_2, NO, N_2O, CO and CO_2)

LIU Chun-Guang* ZHANG Han-Yu JIANG Meng-Xu
(*College of Chemical Engineering, Northeast Electric Power University, Jilin, Jilin* 132012, *China*)

Abstract: Geometries, electronic structure, and bonding nature of a series of mono-manganese-substituted Keggin-type (POMs) with atmospheric small molecules X (X=H_2O, N_2, O_2, NO, N_2O, CO and CO_2) have been studied based on density functional theory (DFT) method with M06L functional. Due to the poly-anionic nature of polyoxometalates (POMs), the counterions effects have firstly been considered by means of a full treatment of the cesium salt $Cs_4[PW_{11}O_{39}Mn^{Ⅲ}H_2O]$. DFT-M06L calculations show that the key geometric a nd electronic parameters are almost constants as change of the four Cs counterions. The optimized calculations for $[PW_{11}O_{39}Mn^{Ⅲ}H_2O]^{4-}$ both in gas phase and solution provide an analogous result, no significant variation of key geometric and electronic parameters was found when compared with the cesium salt. The calculated relative energy of different spin states indicates that the lowest energy spin state is the high-spin quintet state for $[PW_{11}O_{39}Mn^{Ⅲ}X]^{4-}$ (X=H_2O, N_2, N_2O, CO and CO_2), triplet state for $[PW_{11}O_{39}Mn^{Ⅲ}O_2]^{4-}$, and doublet state for $[PW_{11}O_{39}Mn^{Ⅲ}NO]^{4-}$. The calculated adsorption energy of those atmospheric small molecules over the porphyrin-like POM ligand increases in the following order: $N_2<N_2O<CO\approx CO_2<O_2<H_2O<NO$. The Mn-NO POM complex provides considerable adsorption energy. Mulliken population analysis shows that coordination of NO ligand to the $Mn^{Ⅲ}$ center in its doublet ground state arises from an antiferromagnetic coupling between an intermediate-spin $Mn^{Ⅲ}$ center and $NO^{·}$ unit.

Keywords: density functional theory; electronic configuration; polyoxometalates; atmospheric small molecules

收稿日期:2017-10-24。收修改稿日期:2018-02-13。
国家自然科学基金(No.21373043)资助项目。
*通信联系人。E-mail:liucg407@163.com,Tel:+86-432-64606919

0 Introduction

Polyoxometalates (POMs) are early transition metal oxo clusters, which has been widely studied as acid, redox, and bifunctional catalysts in homogeneous as well as in heterogeneous systems[1-6]. An advantage of POM-based catalyst is that they can be designed at atomic or molecular levels based on acidic and redox properties. Many physicochemical behaviors of POMs are now successfully explained on a molecular level because of a careful analysis of both experimental and theoretical data[7-11]. Keggin-type POMs, incorporating one or several transition metals are subjects of active experimental and theoretical research because they serve as structure models for the active sites of oxygenation or acidic catalysts[12-17]. Electronic structure information of these transition-metal-substituted Keggin -type POMs, especially, spin state of the transition metal center, is determining factors for understanding how these POMs perform their catalytic behavior. To date, the accurate determination of the relative energies for the different spin states in the different oxidation states of transition metal center in POM species is still a computational challenge because the theoretical treatment of POMs must take into account several intrinsic difficulties[18-19]. POMs are highly negative charge anionic species, involving multiple transition metal atoms. The highly charge POM anions do not exist in gas phase, and only exist in condensed state because the external field generated from the solvent molecules or the counterions stabilizes POM anions. Most of the theoretical investigations for POMs have been done employing conventional density functional theory (DFT) methods with various XC functional, such as, BP86[20], B3LYP[21], BLYP[13], PBE[22], and M06L[14], *etc*. And the stabilizing fields generated by solvent molecules and counterions were modeled by using continuum model or a set of point charges (modeling the crystal field) [18]. The accuracy and deficiency of these methods are reviewed by Poblet and co-workers[18-19].

Mono-transition-metal-substituted Keggin-type POMs have long been referred to as "inorganic metalloporphyrin" because they have same catalytic behaviors in oxygenation catalysis relevant to metalloporphyrins[23-24]. In particular, a manganese-substituted Keggin-type POMs showed good activity and high selectivity for the epoxidation of alkenes that compared well to the activity of a manganese(Ⅲ) porphyrin[24]. In the past half century, the chemistry of metalloporphyrins has been well studied. It has been found that metalloporphyrins showed highly activity toward oxygen, nitric oxide, carbon monoxide, etc[25-28]. Thus, metalloporphyrins have been considered as potential sensing of gases and catalysts for many important reactions, involving reduction of carbon dioxide, nitrogen oxides, and the oxidation of hydrocarbons and alcohols, *etc*[29-34]. Compared with metalloporphyrins, the inorganic metalloporphyrins with high redox stability can act as a potential multielectron acceptor. Moreover, the unique withdrawing properties of POM ligands would possibly modify the reactivity of the transition metal center. However, the chemistry of "inorganic metalloporphyrin", mono-transition-metal-substituted Keggin-type POMs, is less developed. Under the guidance of porphyrin chemistry and motivated by a theoretical work of abdurahman and co-workers[35], a systematic investigation for the ground state electronic structure, relative spin state energies, and adsorption energies of mono-manganese-substituted Keggin-type POMs with atmospheric small molecules X (X=H_2O, N_2, N_2O, CO and CO_2) has been performed based on DFT calculations. These findings would provide a basis of understanding the structure-property relationships for these "inorganic metalloporphyrin", and be useful to explore the potential applications of POMs in the field of catalytic oxidation of atmospheric small molecules. For modeling of external fields generated by solvent molecules or counterions , the self-consistent reaction field (SCRF) method and a full treatment of the cesium salts $Cs_4[PW_{11}O_{39}Mn^{Ⅲ}X]$ have both been employed in this work.

1 Computational details

All geometric optimizations were performed by

using DFT method with M06L functional. We chose M06L functional[36] because of the proper treatment of transition metal elements and accurate description of non-covalent interactions. Geometric optimization and frequency calculations were used 6-31G (d) basis sets for all main group elements and scalar relativistic effective core potential of LANL2DZ[37-39] for metal atoms. The frequency calculations show that there is no imaginary for all the structures discussed in the present work, which indicates that all of them are minima on the corresponding potential energy surfaces. The adsorption energy (E_{ad}) of the series of atmospheric small molecules X (X=H_2O, N_2, O_2, NO, N_2O, CO and CO_2) over the porphyrin-like POM ligand was calculated by

$$E_{ad}=E_{complex}-(E_{POM}+E_X)$$

where $E_{complex}$, E_{POM}, and E_X are the total energies of the metal-X POM complex, POM fragment, and atmospheric small molecules X, respectively. Bulk solvent effects of acetonitrile media have been taken into account via the SCRF method, using the integral equation formalism polarizable continuum model (IEFPCM) solvent model[40]. All calculations were implemented with the Gaussian 09 package[41].

2 Results and discussion

Due to the poly-anionic nature, counterions are always involved in determination of the structure, reactivity, and physicochemical behavior of POMs both in solid and solution[42-44]. In the present paper, the interaction between Cs counterions and the surface of mono-manganese-substituted Keggin-type POMs may form various structures. However, for large-sized POMs, it is difficult to calculate all possible structures because of the high computational cost. Thus, three typical structural patterns have been considered. A aquamanganese derivative $Cs_4[PW_{11}O_{39}Mn^{Ⅲ}H_2O]$ has been firstly employed as an example to probe effects of Cs counterions. As shown in Fig.1, designed around the surface of POM anion, the average distances among the four Cs counterions are becoming more distant in an order of (a)<(b)<(c). According to our DFT-M06L calculations, the distance of the Cs atom and the nearest O_b atoms of POM anion is in a range of 0.30 ~0.31 nm (O_b corresponds to oxygen atom bridging the two tungsten atoms of the POM unit), which is well in agreement with the experimental values in most typical POM cesium salts[45-47].

The water molecule has the singlet ground state (S=0), and is attached to the POM unit $[PW_{11}O_{39}Mn^{Ⅲ}]^{4-}$ as shown in Fig.1. Thus, the 3d electrons of $Mn^{Ⅲ}$ center have been arranged into three possible spin states, namely, the low-spin state (S=0, M_S=1), intermediate-spin state (S=1, M_S=3), and high-spin state (S=2, M_S=5). The spin multiplicities (M_S=2S+1), key structural parameters, and calculated relative spin-state electronic energies (E_{elec}) and total energies involving electronic and zero-point correction energies ($E_{elec+zero}$), frontier molecular orbital (HOMO and LUMO) energies, HOMO-LUMO energy gap, and spin density of the $Mn^{Ⅲ}$ center (q(Mn)) with M06L functional for the three typical structure of cesium salt $Cs_4[PW_{11}O_{39}Mn^{Ⅲ}H_2O]$ in different spin states are reported in Table 1. For the three structures of cesium salt, all parameters listed in Table 1 are almost not sensitive to the change of arrangement of four Cs counterions according to our DFT-M06L calculations. Both E_{elec} and $E_{elec+zero}$ results indicate that the lowest energy spin state is the high-spin quintet state, and the relative spin-state energy order predicted for those spin states is (S=0)>(S=1)>(S=2) in the three structures of the cesium salt. Meanwhile, a detailed comparison shows that zero-energy correction leads to a slight increase for the relative spin-state energies. Geometrically, in the three structures of cesium salt, the high-spin ground state has the largest Mn-ligand distance, and the order of the Mn-ligand distances for those spin states is (S=2)>(S=1)≈(S=0). By contrast, the average bond length of 4 Mn-O_b bonds ($d_{Mn\text{-}Ob}$) is nearly not affected by the change in the spin state. The order of the HOMO-LUMO gap for those spin states is (S=1)>(S=2)>(S=0). Mulliken spin density calculations for the open-shell species (triplet and quintet states) indicate that unpaired electrons in both spin states are mainly localized on the $Mn^{Ⅲ}$ center in the three structures. No large spin contamination for those spin states was found according to our DFT-M06L calculations.

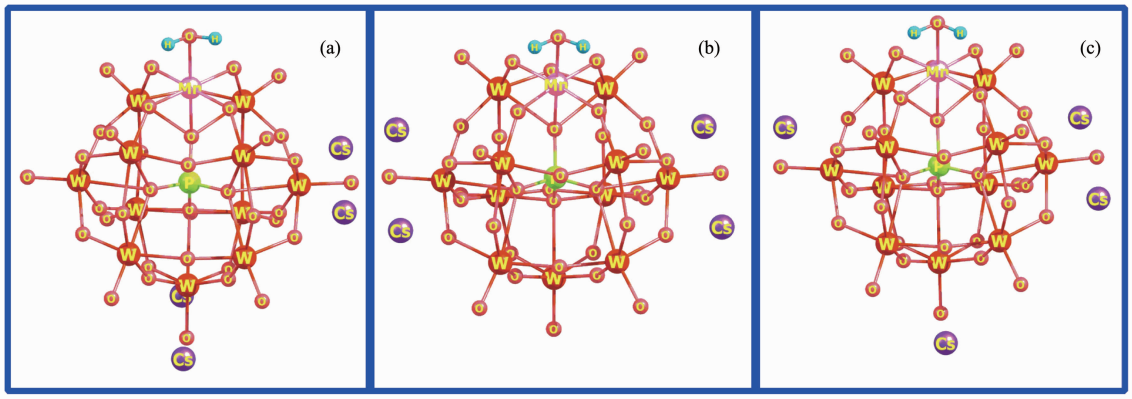

Fig.1 Optimized structures of cesium salt $Cs_4[PW_{11}O_{39}Mn^{III}H_2O]$ obtained by M06L/6-31G(d) calculations (LANL2DZ basis sets on metal atoms)

Table 1 Relative energies (kJ·mol^{-1}), key bond length (nm), frontier molecular orbital energy (eV), and Mulliken spin density (a.u.) for three typical structures of cesium salt, isolated POM anion in acetonitrile solution and gas phase

MS	$<S^2>_C$	$d_{Mn\text{-}H_2O}$ / nm	$d_{Mn\text{-}Ob}$	$d_{Mn\text{-}Oc}$	E_{elec}	$E_{elec+zero}$	HOMO	LUMO	H-L gap	q(Mn)
Cesium salt (a)										
1	0.00	0.206	0.190	0.208	219.07	223.15	−4.216	−3.935	0.282	—
3	2.03	0.204	0.192	0.203	88.78	93.42	−5.105	−2.951	2.155	1.917
5	6.04	0.228	0.191	0.226	0.00	0.00	−5.282	−3.507	1.775	3.800
Cesium salt (b)										
1	0.00	0.206	0.190	0.207	217.40	221.69	−4.181	−3.934	0.247	—
3	2.03	0.205	0.192	0.202	86.41	93.95	−5.126	−2.974	2.152	1.922
5	6.04	0.229	0.191	0.224	0.00	0.00	−5.299	−3.536	1.762	3.804
Cesium salt (c)										
1	0.00	0.205	0.190	0.207	219.32	225.01	−4.295	−4.013	0.283	—
3	2.02	0.204	0.192	0.202	86.38	90.60	−5.195	−3.033	2.162	1.915
5	6.04	0.228	0.191	0.226	0.00	0.00	−5.368	−3.611	1.757	3.801
POM anion in acetonitrile										
1	—*	—*	—*	—*	—*	—*	—*	—*	—*	—*
3	2.04	0.204	0.204	0.202	83.66	94.02	−5.367	−3.207	2.160	1.914
5	6.04	0.227	0.227	0.225	0.00	0.00	−5.449	−3.693	1.756	3.794
Isolated POM anion in gas phase										
1	0.00	0.215	0.215	0.205	227.14	229.33	4.830	5.055	0.225	—
3	2.02	0.212	0.212	0.200	102.59	108.90	3.818	5.932	2.114	1.941
5	6.04	0.265	0.265	0.219	0.00	0.00	3.302	5.430	2.128	3.798

* Optimized geometry of $[PW_{11}O_{39}Mn^{III}H_2O]^{4-}$ has not been achieved because of the bad SCF convergence

The geometry of POM anion $[PW_{11}O_{39}Mn^{III}H_2O]^{4-}$ also has been optimized both in gas phase and acetonitrile at the same levels, respectively. The gas-phase and solvent results for the POM anion $[PW_{11}O_{39}Mn^{III}H_2O]^{4-}$ are also listed in Table 1. It is worth noting that gas-phase calculations for an isolated POM anion is the most popular method that has been used on large POM system at an affordable computational cost in the past two decades. Compared with the full treatment of the cesium salt, there was no significant difference for those parameters except for the FMO energies. It has been demonstrated that the instability of isolated POM anions in gas phase is reflected in the high energy of its molecule orbitals[18].

As shown in Table 1, our DFT-M06L calculations also reproduce this trend. The calculated HOMO and LUMO levels in gas phase lie at positive energies for those spin states. The stabilizing field generated by solvent molecules and counterions significantly decreases the molecular orbital energies, the calculated HOMO and LUMO for these spin states appear at quite negative energies in the three structures of cesium salts and solution. But the relative energies of both orbitals (HOMO-LUMO gaps) in these states do not change largely, such as the calculated HOMO-LUMO gap for the triplet state is 2.11, 2.16, 2.16 eV in gas phase, solution, and cesium salt (b), respectively (Table 1). Due to the low computational cost and reliable electronic and total energy results, the gas-phase calculations will be employed to determine the ground state of the studied POM complexes in the following discussion. Meanwhile, the full treatment of the cesium salt was focused on one structural pattern (c) because those key parameters are almost constant as change of the arrangement of the Cs counterions.

The dinitrogen molecule has a singlet ground state and high chemical inertness. Starting from a linear Mn-N-N arrangement, we performed the geometric optimization of the Mn-dinitrogen POM complex with the three spin states (S=0, M_S=1; S=1, M_S=3; S=2, M_S=5) in gas phase. The predicted lowest energy spin state is the high-spin quintet state (Supporting Information). The molecular geometry of the studied Mn-dinitrogen POM complex the in its quintet ground state was further optimized in acetonitrile and cesium salt at the same levels, respectively. The calculated key geometric and electronic parameters are listed in Table 2 and Fig.2. As shown in Fig.2, our DFT-M06L calculations show a bent Mn-N-N unit a long Mn-ligand distance. The calculated Mn-ligand distance decreases in an order of cesium salt (0.30 nm) > gas phase (0.28 nm) > acetonitrile (0.26 nm), indicating a very weak Mn-dinitrogen interaction both in gas phase and condensed state. Mulliken population analysis shows that the spin density of the Mn-dinitrogen POM complex in the quintet ground state is mainly localized on the $Mn^{Ⅲ}$ center. By contrast, the dinitrogen ligand has very small spin densities.

The ground state of dioxygen molecule is a triplet state with two unpaired elections. In the present paper, we firstly optimized the structure of $[PW_{11}O_{39}Mn^{Ⅲ}O_2]^{4-}$ for the five different spin states (S=0, M_S=1; S=1, M_S=3; S=2, M_S=5; S=3, M_S=7; S=4, M_S=9) in gas phase to determinate the ground state. As a results, the lowest energy spin state is the triplet state (S=1, M_S=3) (Supporting Information). For comparison, the ground state structure was further optimized in acetonitrile and the cesium salt at the same levels, respectively. The calculated key geometric and electronic parameters are also listed in Table 2. It can be found that there are no significant variation of the key geometric and electronic parameters when compared with the gas-phase results. Dioxygen molecule bonding to the Mn center in our studied POM systems leads to a bent Mn-O-O unit with an angle of 117° and a Mn-ligand distance of about 0.20 nm, indicating the dioxygen molecule is loosely bound to the Mn center. Table 2 presents the Mulliken spin densities assigned to the $Mn^{Ⅲ}$ center and dioxygen ligand in its triplet ground state. For all the studied states, about 3.2 unpaired electrons are localized on the $Mn^{Ⅲ}$ center, and about 1.5 unpaired electrons with opposite spin are localized on the dioxygen ligand. Thus, the formation of Mn-dioxygen POM complex in its triplet ground state may be viewed as an antiferromagnetic coupling between a high-spin $Mn^{Ⅲ}$ center and a dioxygen molecule.

NO ligand can be attached to the transition metal center via O- or N-end coordinated models, respectively. In the present paper, we performed the geometric optimization of both coordinated models in the four spin states (S=1/2, M_S=2; S=3/2, M_S=4; S=5/2, M_S=6; S=7/2, M_S=8). The lowest spin state is found to be the doublet state with the N-end coordinated model. The ground state molecular geometry is also optimized in two condensed states. The calculated key geometric and electronic parameters are also listed in Table 2. There are no significant variation of the key geometric and electronic parameters in two condensed

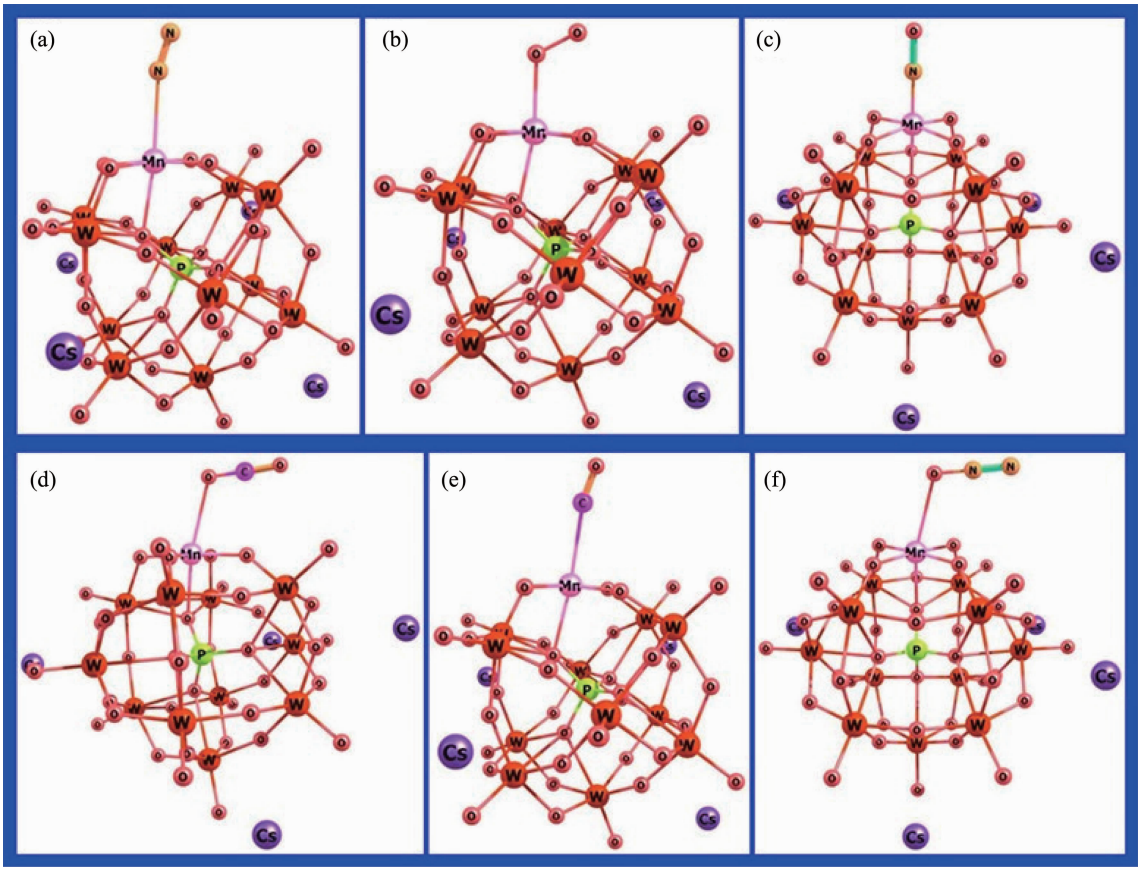

Fig.2 Optimized geometries of $Cs_4[PW_{11}O_{39}Mn^{III}X]$ X=N_2 (a), O_2 (b), NO (c), CO_2 (d), CO (e), N_2O (f) obtained by M06L/6-31G(d) calculations (LANL2DZ basis sets on metal atoms)

Table 2 Key bond length (nm), bond angle (°), and Mulliken spin densities (a.u.) for adsorption complexes studied here (C denoted as cesium salt, S denoted as solution, and G denoted as gas phase)

States	d_{Mn-X}	d_{Mn-Ob}	d_{Mn-Oc}	∠MnX	q(Mn)	q(X)
X=N_2 (Quintet state)						
C	0.258	0.190	0.222	164.9	3.785	−0.001
S	0.304	0.190	0.219	132.4	3.771	0.001
G	0.278	0.190	0.214	135.6	3.760	0.007
X=O_2 (Triplet state)						
C	0.208	0.189	0.220	117.9	3.475	−1.705
S	0.204	0.189	0.216	116.5	3.359	−1.592
G	0.200	0.189	0.213	117.1	3.231	−1.479
X=NO (N-end)(Doublet state)						
C	0.166	0.191	0.211	179.9	1.598	−0.710
S	0.166	0.191	0.209	179.5	1.649	−0.757
G	0.166	0.190	0.208	178.7	1.769	−0.887
X=N_2O (O-end)(Quintet state)						
C	0.253	0.190	0.222	109.0	3.789	0.005
S	0.275	0.190	0.221	103.7	3.783	0.002
G	0.274	0.190	0.216	102.1	3.779	0.001
X=CO (C-end)(Quintet state)						
C	0.250	0.190	0.223	168.2	3.764	0.020

Continued Table 2

S	0.272	0.190	0.221	140.0	3.780	0.004
G	0.266	0.190	0.216	139.7	3.764	0.007
X=CO_2 (Quintet state)						
C	0.251	0.190	0.222	111.7	3.797	0.001
S	0.284	0.190	0.220	101.4	3.789	−0.001
G	0.277	0.190	0.216	96.4	3.790	−0.004

states when compared with the gas-phase calculations. As shown in Fig.2. The optimized calculations show that coordination of NO ligand to the Mn center leads to a linear Mn-N-O unit with an angle of about 179° and a Mn-ligand distance of about 0.166 nm, indicating the formation of a strong Mn-N single bond. The Mn-NO moiety in this Mn-NO POM complex may have various electronic structures, such as, Mn^{II}-$(N\equiv O)^+$, Mn^{III}-$(N=O)^{\cdot}$, and Mn^{IV}-$(N=O)^-$. Table 2 presents the Mulliken spin densities assigned to the Mn^{III} center and NO ligand in its doublet ground state. It can be found that about 1.6 unpaired electrons are localized on the Mn^{III} center, and about 0.8 unpaired electrons with opposite spin are localized on the NO ligand. Thus, coordination of NO ligand to Mn^{III} center in its doublet ground state arises from an antiferromagnetic coupling between an intermediate-spin Mn^{III} center and $NO^{\cdot}$ unit. Therefore, the electronic structure of the Mn-NO moiety of the Mn-NO POM complex in the doublet ground state should be described as Mn^{III}-$(N=O)^{\cdot}$ structure.

N_2O molecule has a linear structure with a singlet ground state. According to literatures, coordination of N_2O molecule to the transition metal center can form metal complexes with O- and N-end models, respectively[48-52]. We considered a bent arrangement of Mn-N_2O unit as the starting geometry and performed the geometric optimization of both coordinated models in the three spin states (S=0, M_S=1; S=1, M_S=3; S=2, M_S=5) based on gas-phase calculations. The optimized calculations show that the lowest energy spin state is the high-spin quintet state with O-end model. Similarly, the molecular geometry of the Mn-N_2O POM complex in its quintet ground state was also optimized in two condensed states. The calculated key geometric and electronic parameters are also listed in Table 2. It can be found that the Mn-ligand distance decreases in an order of acetonitrile (0.27 nm)≈gas phase (0.27 nm)>cesium salt (0.25 nm), which indicates a weak interaction between the N_2O ligand and Mn^{III} center both in gas phase and condensed state. Mulliken population analysis also reflects this weak interaction. The spin density of Mn-N_2O POM complex in its quintet ground state is mainly localized on the Mn^{III} center, and the N_2O ligand has very small spin densities.

Transition metal carbonyl complexes have many types of novel structures because of the variable coordination models of CO ligand. As POM analog, the famous heme-CO systems (an iron porphyrin complex), CO binding to Fe center gives rise to a linear Fe-C-O unit according to many experimental and theoretical studies[53-55]. In the present paper, we considered a similar linear structure as the starting geometry for the Mn-CO POM complex in two coordination models (O- and C-end of CO ligand), and performed the geometric optimization in three spin states (S=0, M_S=1; S=1, M_S=3; S=2, M_S=5) based on gas-phase calculations. According to our DFT-M06L calculations, the lowest energy spin state is the high-spin quintet state with the C-end coordination model. As before, the ground state molecular geometry of the Mn-CO POM complex was optimized in acetonitrile and the cesium salt at the same levels, respectively. The calculated key geometric and electronic parameters also listed in Table 2 and Fig.2. As shown in Fig.2, our DFT-M06L calculations show a bent Mn-C-O unit with a long Mn-ligand distance. The optimized Mn-ligand distance decreases in an order of acetonitrile (0.27 nm)≈gas phase (0.27 nm)>cesium salt (0.25 nm), indicating a weak interaction between Mn^{III} center and the CO ligand both in gas phase and condensed state. The Mulliken popula-

tion analysis also supports this results, where the spin density of the studied Mn-CO POM complex in its quintet ground state is mainly localized on the Mn^{III} center, and the CO ligand has hardly any spin densities.

CO_2 is a tri-atomic molecule with a linear structure. Due to the different electronegativities, the carbon atom in CO_2 molecule carries partial positive charge and the oxygen atom in CO_2 molecule carries partial negative charge. It is known that CO_2 molecule has two set of π molecular orbitals in its singlet ground state. And both sets of π molecular orbitals are orthogonal to each other. These structural features result in variable coordination models of CO_2 ligand when interacting with transition metal centers. In the present paper, starting from various structures, including linear, bent, O-end, and C-end structures, we performed geometric optimization in three spin states (S=0, M_S=1; S=1, M_S=3; S=2, M_S=5) based on gas-phase calculations. Interestingly, all those optimized calculations provide the same structure as shown in Fig.2. CO_2 molecule is attached to the Mn^{III} center as a bent arrangement via a very weak interaction in their O-end coordination models, According to our DFT-M06L calculations, the lowest energy spin state is the high-spin quintet state. The molecular geometries of the studied Mn-CO_2 POM complex in its quintet ground state was further optimized in acetonitrile and cesium salt at the same levels, respectively. All the optimized calculations show a long Mn-ligand distance. As shown in Table 2, the optimized Mn-ligand distance decreases in an order acetonitrile (0.28 nm) ≈ gas phase (0.28 nm) > cesium salt (0.25 nm). Mulliken population analysis also supported this weak interaction. The spin density of the studied Mn-CO_2 POM complex in its quintet ground state is mainly localized on the Mn^{III} center. There are nearly no spin densities on CO_2 ligand in its quintet ground state.

On the basis of the optimized geometries in their ground states, the adsorption energy (E_{ad}) of atmospheric small molecules X (X=H_2O, N_2, O_2, NO, N_2O, CO, and CO_2) over the porphyrin-like POM ligand was calculated in gas phase, acetonitrile, and cesium salt, respectively. The calculated E_{ad} values were listed in Table 3. It can be found that the solvent calculations for each POM complex studied here provided a low adsorption energy when compared with the results derived from gas phase and a full treatment with the cesium salts. All DFT-M06L calculations indicate the adsorption energy of the POM complexes studied here increases in the following order: N_2<N_2O<CO ≈ CO_2< O_2<H_2O<NO, especially, the Mn-NO POM complex provides considerable adsorption energy of −199.6, −175.5, and −206.5 kJ·mol^{-1} in gas phase, acetonitrile, and cesium salt, respectively. This result is well in agreement with the prediction based on their molecular geometries, a strong Mn-N single bond.

Table 3 Calculated adsorption energies (kJ·mol^{-1}) for the series of POM complexes in gas phase, acetonitrile, and cesium salt obtained by M06L/6-31G(d) calculations (LANL2DZ basis sets for metal atoms)

X	Gas phase	Acetonitrile	Cesium salt
H_2O	−88.36	−55.82	−87.81
N_2	−20.58	−10.45	−24.72
O_2	−60.28	−26.49	−40.12
NO	−199.62	−175.49	−206.48
N_2O	−33.96	−13.28	−34.21
CO	−35.40	−18.20	−40.71
CO_2	−38.79	−17.76	−29.44

3 Conclusions

We have performed DFT calculations to study molecular geometries and electronic structures of a series of Mn-POM complexes [$PW_{11}O_{39}Mn^{III}X$], which are generated by coordination of atmospheric small molecule X (X=H_2O, N_2, O_2, NO, N_2O, CO and CO_2) to

the $Mn^{Ⅲ}$ center. Because those Mn-POM complexes carry highly negative charge, we firstly explored the counterions effects by means of a full treatment of the cesium salt $Cs_4[PW_{11}O_{39}Mn^{Ⅲ}H_2O]$. Three typical structure patterns of the cesium salt, which were differentiated by the average distances among the four Cs counterions around the surface of POM anion, were considered in the present work. According to our DFT-M06L calculations, the key geometric and electronic parameters are almost constants as change of the average distances of the four Cs counterions. For comparison, molecular geometry of $[PW_{11}O_{39}Mn^{Ⅲ}H_2O]^{4-}$ was also optimized in both gas phase and acetonitrile. Optimized calculations show that there are no significant variation of the key geometric and electronic parameters when compared with the full treatment of the cesium salt. DFT-derived relative energy of different spin states reveal that the lowest energy spin state is the high-spin quintet state for $[PW_{11}O_{39}Mn^{Ⅲ}X]^{4-}$ ($X = H_2O$, N_2, N_2O, CO, and CO_2), triplet state for $[PW_{11}O_{39}Mn^{Ⅲ}O_2]^{4-}$, and doublet state for $[PW_{11}O_{39}Mn^{Ⅲ}NO]^{4-}$, respectively. Our DFT-M06L calculations indicate that the adsorption energy of those atmospheric small molecules over the porphyrin-like POM ligand increases in the following order: $N_2<N_2O<CO\approx CO_2<O_2<H_2O<NO$. Mulliken population analysis shows that coordination of NO ligand to $Mn^{Ⅲ}$ center in its doublet ground state arises from an antiferromagnetic coupling between an intermediate-spin $Mn^{Ⅲ}$ center and NO^- unit.

Supporting information is available at http://www.wjhxxb.cn

References:

[1] Kozhevnikov I V. *Chem. Rev.*, **1998**,**98**:171-198

[2] Weinstock I A. *Chem. Rev.*, **1998**,**98**:113-170

[3] Mizuno N, Misono M. *Chem. Rev.*, **1998**,**98**:199-218

[4] Dolbecq A, Dumas E, Mayer C R, et al. *Chem. Rev.*, **2010**, **110**:6009-6048

[5] Sun M, Zhang J, Putaj P, et al. *Chem. Rev.*, **2014**,**114**:981-1019

[6] Wang S S, Yang G Y. *Chem. Rev.*, **2015**,**115**:4893-4963

[7] Vilà-Nadal L, Mitchell S G, Rodríguez-Fortea A, et al. *Phys. Chem. Chem. Phys.*, **2011**,**13**:20136-20145

[8] Vilà-Nadal L, Mitchell S G, Long D L, et al. *Dalton Trans.*, **2012**,**41**:2264-2271

[9] McGlone T, Vilà-Nadal L, Miras H N, et al. *Dalton Trans.*, **2010**,**39**:11599-11604

[10]Rubinstein A, Jiménez-Lozanao P, Carbó J J, et al. *J. Am. Chem. Soc.*, **2014**,**136**:10941-10948

[11]Marrot J, Pilette M A, Haouas M, et al. *J. Am. Chem. Soc.*, **2012**,**134**:1724-1737

[12]FAN Ying(樊莹), LIU Shi-Zhong(柳士忠). *Chinese J. Inorg. Chem.*(无机化学学报), **2002**,**18**:635-638

[13]Khenkin A M, Kumar D, Shaik S, et al. *J. Am. Chem. Soc.*, **2006**,**128**:15451-15460

[14]Liu C G, Liu S, Zheng T. *Inorg. Chem.*, **2015**,**54**:7929-7935

[15]Liu C G, Su Z M, Guan W. *Inorg. Chem.*, **2009**,**48**:541-548

[16]Liu C G, Guan W, Yan L K, et al. *Dalton Trans.*, **2011**,**40**: 2967-2974

[17]Liu C G, Guan W, Yan L K, et al. *Dalton Trans.*, **2009**,**38**: 6208-6213

[18]Poblet J M, López X, Bo C, et al. *Chem. Soc. Rev.*, **2003**, **32**:297-308

[19]López X, Carbó J J, Bo C, et al. *Chem. Soc. Rev.*, **2012**,**41**: 7537-7571

[20]Maestre J M, López X, Bo C, et al. *J. Am. Chem. Soc.*, **2001**, **123**:3749-3758

[21]Antonova N S, Carbó J J, Kortz U, et al. *J. Am. Chem. Soc.*, **2010**,**132**:7488-7497

[22]Efremenko I, Neumann R. *J. Am. Chem. Soc.*, **2012**,**134**: 20669-20680

[23]Hill C L, Brown R B. *J. Am. Chem. Soc.*, **1986**,**108**:536-538

[24]Mansuy D, Bartoli J F, Battioni P, et al. *J. Am. Chem. Soc.*, **1991**,**113**:7222-7226

[25]Karpuschkin T, Kappes M M, Hampe O. *Angew. Chem. Int. Ed.*, **2013**,**52**:10374-10377

[26]Chen O, Groh S, Liechty A, et al. *J. Am. Chem. Soc.*, **1999**, **121**:11910-11911

[27]Kano K, Itoh Y, Kitagishi H, et al. *J. Am. Chem. Soc.*, **2008**, **130**:8006-8015

[28]Wasser I M, Huang H W, Moenne-Loccoz P, et al. *J. Am. Chem. Soc.*, **2005**,**127**:3310-3320

[29]Morris A J, Meyer G J, Fujita E. *Acc. Chem. Res.*, **2009**,**42**: 1983-1994

[30]Groves J T, Roman J S. *J. Am. Chem. Soc.*, **1995**,**117**:5594-5595

[31]Saito S, Ohtake H, Umezawa N, et al. *Chem. Commun.*, **2013**,**49**:8979-8981

[32]Phougat N, Vasudevan P, Jha N K, et al. *Transition Metal Chem.*, **2003**,**28**:838-847

[33]Meunier B. *Chem. Rev.*, **1992**,**92**:1411-1456

[34]Liu L, Yu M, Wayland B B, et al. *Chem. Commun.*, **2010**, **46**:6353-6355

[35]Abdurahman A, Renger T. *J. Phys. Chem. A*, **2009**,**113**: 9202-9206

[36]Zhao Y, Truhlar D G. *J. Chem. Phys.*, **2006**,**125**:1-18

[37]Hay P J, Wadt W R. *J. Chem. Phys.*, **1985**,**82**:270-283

[38]Wadt W R, Hay P J. *J. Chem. Phys.*, **1985**,**82**:284-293

[39]Hay P J, Wadt W R. *J. Chem. Phys.*, **1985**,**82**:299-310

[40]Tomasi J, Mennucci B, Cammi R. *Chem. Rev.*, **2005**,**105**: 2999-3093

[41]Frisch M J, Trucks G W, Schlegel H B, et al. *Gaussian, Inc., Wallingford CT*, **2009**, *Gaussian* 09, *Revision* D.01

[42]Kirby J F, Baker L C W. *Inorg. Chem.*, **1998**,**37**:5537-5543

[43]Brevard C, Schimpf R, Tourne G, et al. *J. Am. Chem. Soc.*, **1983**,**105**:7059-7063

[44]Grigoriev V A, Cheng D, Hill C L, et al. *J. Am. Chem. Soc.*, **2001**,**123**:52925307

[45]Kato C N, Kashiwagi T, Unno W, et al. *Inorg. Chem.*, **2014**, **53**:4824-4832

[46]Mizuno N, Min J S, Taguchi A. *Chem. Mater.*, **2004**,**16**: 2809-2825

[47]Bi L H, Reicke M, Kortz U, et al. *Inorg. Chem.*, **2004**,**43**: 3915-3920

[48]Pamplin C B, Ma E S F, Safari N, et al. *J. Am. Chem. Soc.*, **2001**,**123**:8596-8597

[49]Groves J T, Roman J S. *J. Am. Chem. Soc.*, **1995**,**117**:5594-5595

[50]Groves J T, Quinn R. *J. Am. Chem. Soc.*, **1985**,**107**:5790-5791

[51]Ben-Daniel R, Weiner L, Neumann R. *J. Am. Chem. Soc.*, **2002**,**124**:8788-8789

[52]Ghosh A. *Acc. Chem. Res.*, **2005**,**38**:943-954

[53]Kachalova G S, Pepov A N, Bartunik H D. *Science*, **1999**, **284**:473-476

[54]Spiro T G, Kozlowski P M. *J. Am. Chem. Soc.*, **1998**,**120**: 4524-4525

[55]Rovira C, Kunc K, Hutter J, et al. *Int. J. Quantum Chem.*, **1998**,**69**:31-35